Title
Membraneless laminar flow cell for electrocatalytic CO2 reduction with liquid product separation

Journal
Journal of Physics D, 50(15)

ISSN
0022-3727

Authors
Monroe, Morgan M
Lobaccaro, Peter
Lum, Yanwei
et al.

Publication Date
2017-04-20

DOI
10.1088/1361-6463/aa6359

Peer reviewed

Membraneless Laminar Flow Cell for Electrocatalytic CO_2 Reduction with Liquid Product Separation

Morgan M. Monroe,[1,2,3] **Peter Lobaccaro,**[1,2] **Yanwei Lum,**[1,3] **and Joel W. Ager**[1,3,4*]

[1]Joint Center for Artificial Photosynthesis, Lawrence Berkeley National Laboratory, Berkeley, CA, USA

[2]Department of Chemical and Biomolecular Engineering, University of California, Berkeley, CA, USA

[3]Department of Materials Science and Engineering, University of California Berkeley, Berkeley, CA, USA

[4]Materials Sciences Division, Lawrence Berkeley National Laboratory, Berkeley, CA, USA

*E-mail: JWAger@lbl.gov

Abstract.

The production of liquid fuel products via electrochemical reduction of CO_2 is a potential path to produce sustainable fuels. However, to be practical, a separation strategy is required to isolate the fuel-containing electrolyte produced at the cathode from the anode and also prevent the oxidation products (i.e. O_2) from reaching the cathode. Ion-conducting membranes have been applied in CO_2 reduction reactors to achieve this separation, but they represent an efficiency loss and can be permeable to some product species. An alternative membraneless approach is developed here to maintain product separation through the use of a laminar flow cell. Computational modelling shows that near-unity separation efficiencies are possible at current densities achievable now with metal cathodes via optimization of the spacing between the electrodes and the electrolyte flow rate. Laminar flow reactor prototypes were fabricated with a range of channel widths by 3D printing. CO_2 reduction to formic acid on Sn electrodes was used as the liquid product forming reaction, and the separation efficiency for the dissolved product was evaluated with high performance liquid chromatography. Trends in product separation efficiency with channel width and flow rate were in qualitative agreement with the model, but the separation efficiency was lower, with a maximum value of 90% achieved.

1. Introduction

The increasing rate of anthropogenic CO_2 emission into the Earth's atmosphere and the resulting climate change effects [1] have sparked considerable interest in developing renewable energy sources that do not further disrupt the carbon cycle [2–5]. The direct generation of chemical fuels from sunlight, known as "artificial photosynthesis," is one such approach [6–9]. Photoelectrochemical (PEC) production of hydrogen via water splitting has been extensively investigated [10–12] using a number of device geometries [13]. Solar to hydrogen conversion efficiencies of up to 15% (and up to 30% with solar concentration) have been reported [14–17], although the overall cost and durability of such systems remain a concern [18–23].

It is conceptually very attractive to produce carbon-based fuels directly from sunlight, CO_2, and water, analogous to natural photosynthesis. Such a system could conceivably lead to a closed carbon cycle and arrest the current trend of climate change [24]. Realizing such a system entails a number of challenges [25–27], including the development of electrocatalysts which can selectively produce desired fuel chemicals such as methanol and ethanol [28–32]. The system and catalyst deficiencies have resulted in demonstrated free energy conversion efficiencies for solar-driven CO_2 reduction devices lower than that for water splitting, with the highest reports in the range of 5-10% [33–35]. Moreover, with only a few exceptions [36], these types of solar-driven devices produce either CO or formate ($HCOO^-$), both of which would require further processing to be usable as a fuel, further reducing the overall energy conversion efficiency of the system [37].

In contrast to some solar to hydrogen demonstrations [38,39], collection of a usable fuel product in either a PEC or EC CO_2 reduction system has not been convincingly demonstrated. Product separation is a key delineating factor. For solar water splitting the product H_2 is not soluble in the electrolyte and thus can be collected as it outgasses. To keep this H_2 stream pure, a number of systems have used a proton conducting membrane between the cathode and anode chambers to prevent gas crossover from the anode [40]. The situation with EC or PEC CO_2 reduction is considerably more challenging. Insoluble gas products produced, such as CO, CH_4, and C_2H_4, will outgas similar to H_2, but will be entrained with the CO_2 used to feed the cell. Moreover, the liquid products produced, such as formate and ethanol, are soluble in the aqueous electrolyte. Similar to the water splitting system, a membrane can be employed to separate the products made at the cathode from the anode [41–43]. This is especially important to prevent the soluble products from crossing over to the anode where they can be re-oxidized, in most cases more easily than

water. However, the cation and anion-conducting membranes typically used in research cells can allow some of these liquid products to permeate [41–43], so they do not represent an ideal solution.

The product separation requirement in EC CO_2 reduction systems is analogous with the requirement for reactant and oxidant separation in fuel cells. Ion-selective membranes are commonly used for this purpose; however, performance limitations can arise due to water management, reactant crossover, and membrane degradation [44]. For this reason, there has been considerable research on developing fuel cell designs that maintain reactant and oxidant separation without the use of a membrane. In particular, the use of co-laminar flow [45,46], often in a microfluidic geometry [47], has been explored by a number of research groups. Kjeang *et al*. provide a recent review of work in this area [48].

There has been some work in adapting concepts from membraneless fuel cells to EC CO_2 reduction. Kenis and co-workers [49–52] have used a laminar flow channel in combination with a gas-diffusion electrode in their studies of high current density CO_2 reduction. While in their earlier reports product separation was not specifically addressed, in their most recent work an anion conducting membrane is used to prevent product crossover [52]. In this work, we examine the feasibility of using a co-laminar flow geometry to affect efficient separation of liquid product streams in aqueous electrochemical CO_2 reduction. Formate ($HCOO^-$) was used as the model liquid product as selective catalysts (e.g. Sn, In) are available for its production [53]. Also, in the 2 electron electrochemical reduction of CO_2 to $HCOO^-$ in water no known stable intermediates have either been proposed or experimentally observed [32,54–56]; modeling of reactions with intermediates which could desorb from the cathode would require a more sophisticated model. Modeling of the design geometry was used to identify the key factors influencing the efficiency of product separation. Finally, prototype devices were fabricated with 3-D printing and the product separation efficiency for CO_2 reduction to formate on Sn electrodes was measured experimentally for a number of cell geometries and electrolyte flow rates. In general, the observed product distribution was lower than that predicted by the model, although separation efficiencies up to 90% were experimentally achieved.

2. Methodology

Design overview

A top-view schematic of the co-laminar flow reactor used in this work is shown in Fig. 1. It is conceptually similar to the laminar flow fuel cell investigated by Chang *et al.* [57] although the direction of the fluid flow is reversed. CO_2-saturated water enters the cell at the bottom and flows past the cathode and anode, which produce formate ions and O_2, respectively, via reactions (1) and (3). The conditions for CO_2 reduction at the cathode also make reaction (2), hydrogen evolution, possible as a parasitic loss. At the end of the reaction channel there is a Y-split. Provided the reduced product does not diffuse across the midline of the device, and laminar flow is maintained, the formate ion product exits through the cathode channel. Product that diffuses across the mid-line exits through the anode channel and would represent a separation efficiency loss.

$$CO_2 + H_2O + 2e^- \Leftrightarrow OH^- + HCOO^- \quad (1)$$

$$2H^+ + 2e^- \Leftrightarrow H_2(g) \quad (2)$$

$$H_2O \Rightarrow \frac{1}{2}O_{2(g)} + 2H^+ + 2e^- \quad (3)$$

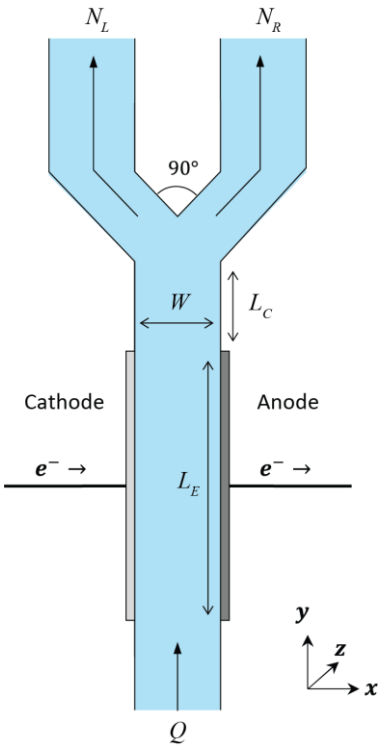

Figure 1. Cross section view of the Y-channel geometry of the laminar CO_2 reduction flow cell. CO_2 saturated water enters at the bottom of the device at flow rate Q. Liquid products are generated at the cathode and O_2 is generated at the anode via water oxidation. The Y-split at top of the figure divides the flow into two channels; reduced products are concentrated in the left-hand (cathode) channel.

Table 1. Variables used in the simulations of fluid flow and convection-diffusion transport of formate in a co-laminar CO_2 reduction flow cell.

Variable	Description (units)	Value
D_{CO_2}	Diffusion coefficient of CO_2 (m^2 s^{-1})	1.91×10^{-9}
D_{HCOO^-}	Diffusion coefficient of formate ion (m^2 s^{-1})	1.45×10^{-9}
H	Channel height (m)	5×10^{-3} (fixed)
J_L	Net $HCOO^-$ flux from left outlet (mol s^{-1})	calculated
J_R	Net $HCOO^-$ flux from right outlet (mol s^{-1})	calculated
L	Channel length (m)	$L_E + L_C$
L_E	Electrode length (m)	varied
L_C	Connector length (m)	$L - L_M$
N_L	Molar flux from left outlet (mol m^{-2} s^{-1})	calculated
N_R	Molar flux from right outlet (mol m^{-2} s^{-1})	calculated
Q	Fluid flow rate (m^3 s^{-1})	varied
Re	Reynolds number	calculated
t_{diff}	Characteristic diffusion time (s)	calculated
t_{res}	Residence time in reaction zone (s)	calculated
W	Channel width (m)	varied
η	Fluid dynamic viscosity (kg m^{-1} s^{-1})	8.90×10^{-4}
ρ	Fluid density (kg/m^3)	10^3

The analysis developed by Goulet *et al.* for a similar co-laminar fuel cell was used as a starting point for the design [58]. The channel height H was fixed uniformly at 5 mm for all simulations; due to the symmetry of the system, this variable would not be expected to influence the design considerably. A first design constraint is a sufficiently low Reynolds number ($Re < 1000$) to ensure fully laminar flow in all regions of the channel. This places an upper limit on the fluid velocity U which can be used:

$$Re = \frac{\rho U W}{\eta} \leq 1000\ . \tag{3}$$

For channel widths W in the range of 5-20 mm, this constrains U to less than 0.18 m s^{-1} for a 5 mm channel and 0.045 m s^{-1} for a 20 mm channel (for the 5 mm channel height assumed here these limits correspond to a flow rate of 270 ml min^{-1}, which is significantly higher than the range experimentally employed). The second constraint is that the residence time t_{res} in the product-forming portion of the channel be less than the diffusion time for crossover of a reduced species to the opposite electrode t_{diff}, as described in Eqn. (4) [59]:

$$t_{res} = \frac{L}{U} < \frac{W^2}{2D} = \overline{t_{diff}}\ . \tag{4}$$

Equation (4) can be used to form a dimensionless relation that balances the convective and diffusive transport terms relevant for laminar flow systems (Eqn. 5). This relation was used to define a set of cell dimensions for which the crossover of reacting species is minimized.

$$\frac{Q\,W}{2\,D\,H\,L} > 1. \tag{5}$$

As an example, Equation (5) yields 785 for a channel width W = 15 mm and a flow rate of 3 cm^3 min^{-1}. We note that while it would have been desirable to set L_C, the connector section of the channel before the Y-split with no flux of formate from the cathode, to zero, it was not possible to fabricate a functional cell in this manner.

The separation efficiency, i.e. the proportion of reduced product exiting the left-hand channel versus the right-hand channel, was used as the figure of merit.

$$\text{Separation efficiency} = 100\% * \left(\frac{J_L}{J_R + J_L}\right) \tag{6}$$

This value approaches 100% for efficient separation and is 50% for inefficient (i.e. no) product separation. For comparison to experimental measurements, the selectivity and activity of the cathode materials and the detection limits of the product analysis tool should be considered. As discussed in the Supplementary Information (SI), the detection limit for formate for the high performance liquid chromatogram (HPLC) was on the order of 0.1 mM. The average concentration in the channel, assuming 100% faradaic efficiency (FE), is

$$\frac{J_{cathode}\,H\,L}{2\,F\,Q}, \tag{7}$$

where F is Faraday's constant. As an example, for a current density of 5 mA cm^{-2} at the cathode and an electrode length of 50 mm, the predicted average formate concentration for Q = 10 ml min^{-1} is 0.4 mM. While this is higher than the detection limit, we found that the fact that the actual FE was less than 100% (see below) and the noise floor on the formate determination in the right hand (anode) channel limited the accuracy of the separation measurement at high flow rates.

System Modelling

The laminar flow physics model in COMSOL was used to model the bulk flow of CO_2 saturated H_2O. The system was assumed to be in steady state with an incompressible fluid flowing at a set inlet flowrate. The system was modeled in two dimensions as it was assumed that the channel height, being similar to the widths considered, was sufficient for fully developed flow in the channel. A no-slip condition was assumed along the channel walls and an open boundary

condition was assumed at the outlet ports. The domain material was assumed to have the same properties as deionized water, and chemical reactions occurring in the channel were assumed to have negligible effects on the fluid dynamic properties of the system. Once implemented, this part of the calculation produced a vector field for the fluid velocity across the entire sample volume (Fig. S1). As expected, the flow was laminar and the velocity profile reached its fully developed form within a few mm of the inlet (Fig. S1b). This allowed simpler versions of the model to be used for some of the calculations.

The transport of dilute species package in COMSOL was used to model consumption of CO_2 at the cathode via reaction (1). The solution at the inlet was CO_2-saturated 0.1 M KCO_3 buffer, pH 6.8 [60]. The inlet (bulk) concentration of $HCOO^-$ was assumed to be zero. A fixed current density of 5 mA cm^{-2} was assumed for the cathode producing 100% FE to formate, using a channel height of 5 mm. This value was chosen as Sn has been reported to have a high faradaic efficiency for formate at this current density [53]. In initial studies, the homogeneous reactions of CO_2 with HCO_3^-, CO_3^{2-}, and OH^-/H^+ (7) were also modeled using diffusion coefficients and rate constants from Gattrell and co-workers [61]:

$$CO_{2\,(aq)} + H_2O \overset{K_1}{\Leftrightarrow} H^+_{(aq)} + HCO^-_{3\,(aq)} \overset{K_2}{\Leftrightarrow} 2H^+_{(aq)} + CO^{2-}_{3\,(aq)} \quad (7)$$

However, we found that the incorporation of the bicarbonate buffer equilibrium system into the model, while dramatically increasing the time needed to perform the calculation, did not significantly affect the results. As such, a simpler model was implemented which considered only the consumption of the CO_2 reaction and the production of $HCOO^-$ [56], both of which were subject to convection and diffusion in the channel.

Formate production at the cathode, reaction (1), is in competition with H_2 evolution, reaction (2). The surface concentration of CO_2 at the cathode should not become too low; otherwise H_2 evolution will be favored and the FE for formate production will decline. We estimated the minimum concentration required to maintain a dominant rate of reaction (1) by calculating the CO_2 profile for a flat electrode in a stirred reactor with a 100 μm boundary layer, which corresponds to the conditions used in 3-electrode measurements. This analysis led to an estimate of 10 mM, which can be compared to the bulk concentration of CO_2 in water saturated at 1 atm, 33.4 mM. We then used the model for the reactor to determine minimum flow rates necessary to maintain the surface CO_2 concentration at or above the minimum value. Fig 2(a) shows a typical CO_2 concentration contour plot for a flow rate Q = 10 ml min^{-1} and W = 15 mm, and Fig 2(b)

shows the CO_2 concentration as a function of distance into the reactor at the cathode surface, 100 μm from the cathode, and at the midline of the reactor. The depletion in CO_2 concentration down the length of the reactor, and the increase in surface CO_2 concentration after transit past the end of the reaction zone can been seen. Figure 2(c) shows the minimum CO_2 surface concentration rate as a function of flow rate for a range of channel widths.

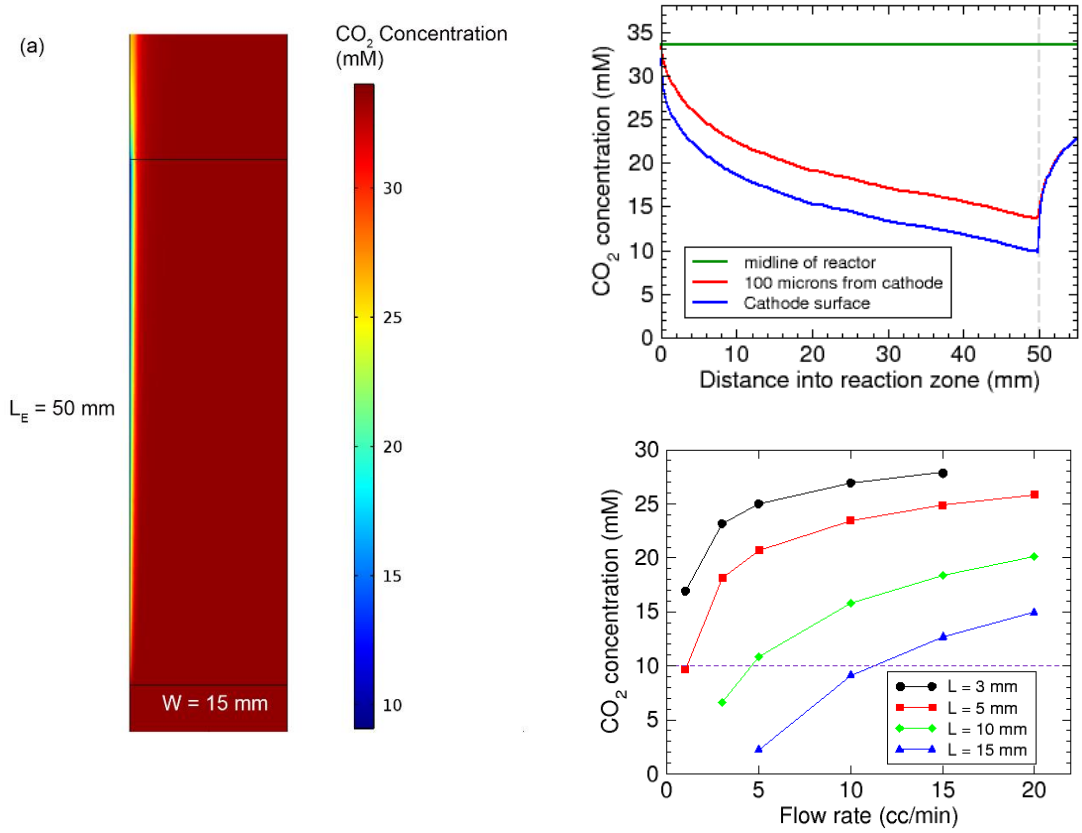

Figure 2. (a) Calculated CO_2 concentration for W = 15 mm, L_E = 50 mm, and Q = 10 ml min^{-1}. A cathode current density of 5 mA cm^{-2} was assumed. (b) CO_2 concentration at the electrode surface, 100 mm from the electrode, and at the midline of the reactor for the simulation shown in (a). (c) Minimum surface CO_2 concentration as a function of flow rate for 4 values of the channel width W. A surface concentration of 10 mM, which we estimate to be required to favor $HCOO^-$ over H_2 formation, is indicated with a dashed line.

With the parameters needed to maintain the CO_2 supply established, the separation efficiency can be modelled. The product flow in the device was evaluated from the molar flux, which is the product of the velocity and the formate concentration. This value, integrated across the dimensions of the outlets, was used to calculate the separation efficiency, Eqn. (6). Two extreme cases of product separation are shown in Fig 3. In Fig. 3(a), efficient (>99 %) separation efficiency is predicted with a relatively wide channel (10 mm) and fast flow (5 ml min^{-1}). In contrast, Fig. 3(b)

depicts a situation with poorer separation (91%) from a simulation with a narrow channel (2 mm) and slow flow (1 ml min^{-1}).

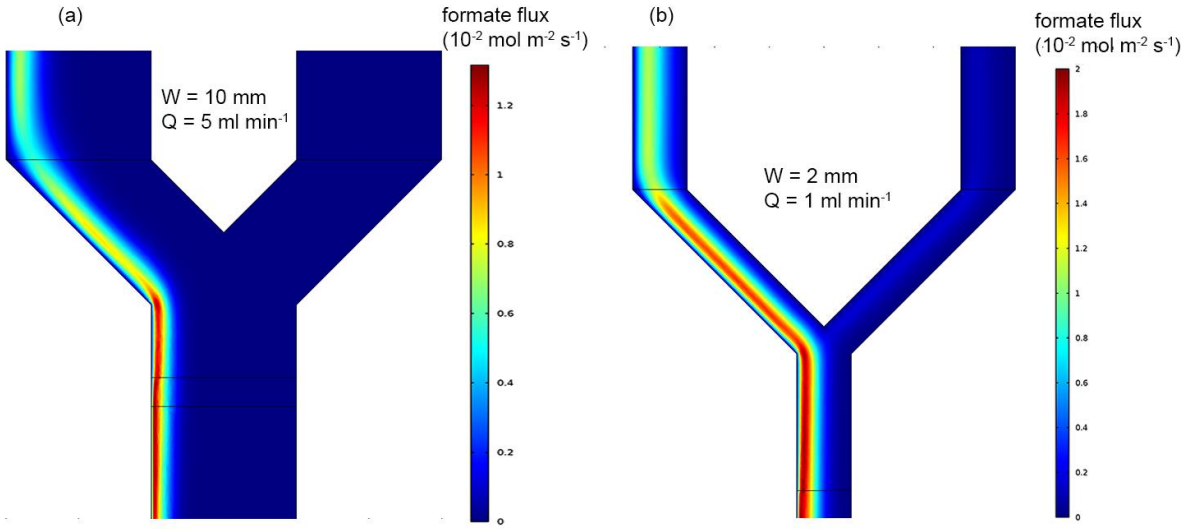

Figure 3. Examples of efficient (a) and inefficient (b) product separation in a laminar flow CO_2 reduction reactors. The contours show molar fluxes in units of 10^{-2} mol m^{-2} s^{-1}. The parameters for (a) are W = 10 mm, L_E = 50 mm, and Q = 5 mL min^{-1}. The parameters for (b) are W = 2 mm, L_E = 50 mm, and Q = 1 mL min^{-1}. For both cases, H = 5 mm and L_C = 5 mm. A current density of 5 mA cm^{-2} was assumed. In (a), the separation efficiency is essentially 100%; in (b) it is 91.5%.

The simulation was used to calculate the dependence of the product separation efficiency on the design parameters most relevant to the fabrication and operation of a prototype cell: electrode length L_E, the connector length L_C, the channel width W, and the inlet flow rate Q. Selected results from this analysis are shown graphically in Fig. 4. As expected, it was found that increases in channel width or flow rate increased the product separation efficiency.

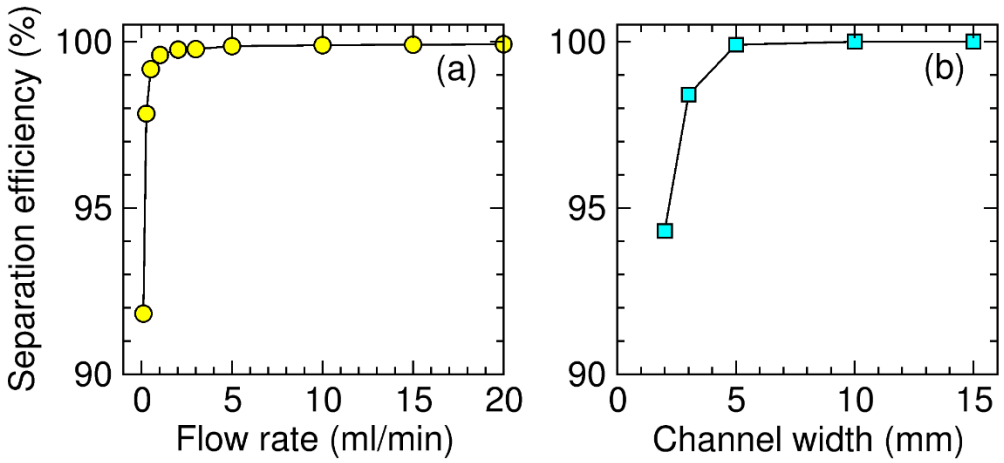

Figure 4. Modeling of membraneless co-laminar CO_2 reduction flow separation efficiencies as a function of physical variables. (a) Flow rate varied at fixed W = 5 mm (b) Channel width varied at Q = 5 ml min^{-1}. For both (a) and (b) L_E = 50 mm, and L_C = 5 mm.

Prototype Cell Fabrication and Operation

Based on the modeling and simulation, three prototypes with width W = 5, 10, and 15 mm with a fixed electrode length L_E = 50 mm were constructed by 3D printing using a Stratasys printer with Fullcure 720 translucent polymer printing material. Figure 5 shows a CAD schematic of the design. The high purity Sn foil cathode and Pt foil counterelectrode were clamped to the device with the seal provided by a silicone gasket. The surface finish provided by the 3D printer was an important experimental parameter and some additional machining of the surfaces was required to obtain a water-tight seal.

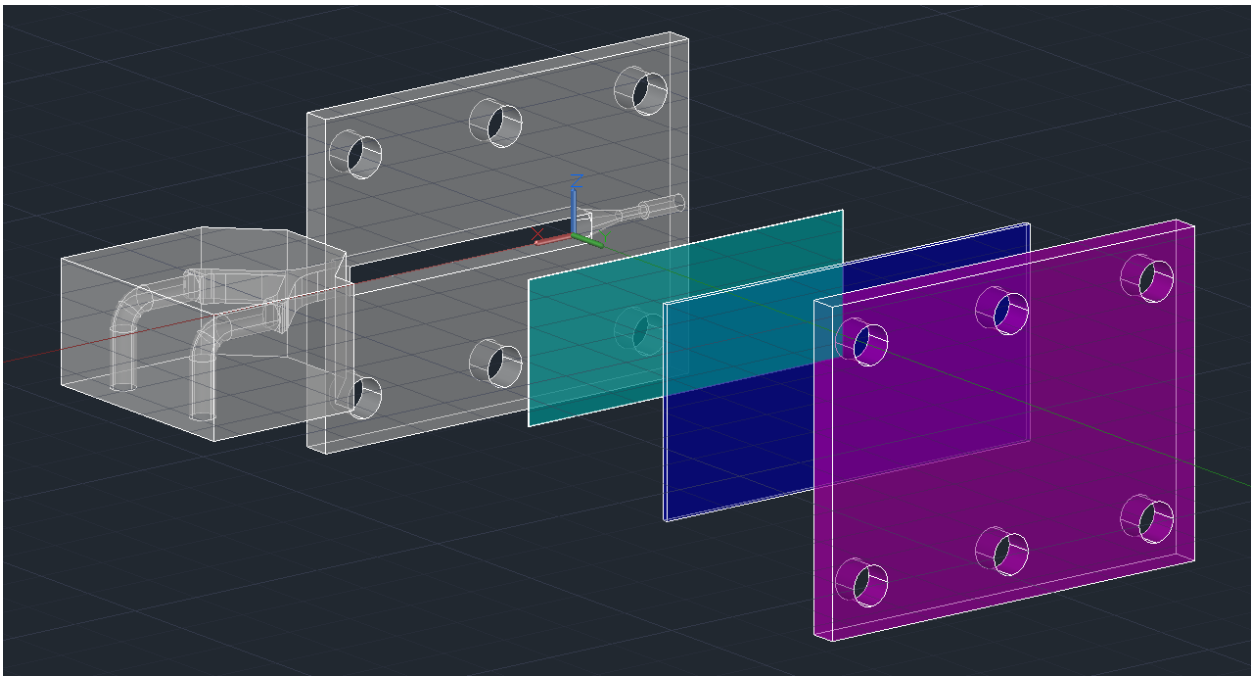

Figure 5. CAD schematic of a laminar flow reactor prototype with W = 5 mm showing one half of the stack. A metal foil catalyst (teal) was aligned with an opening in the channel, then sealed using a silicone gasket (blue) and compressed with a rigid plastic endplate (purple). A symmetric assembly was implemented for the reverse side of the device (not shown)

Cell operation procedure

A 0.05M K_2CO_3 (99.997% Alfa Aesar) solution was presaturated with CO_2 to produce 0.1 M $KHCO_3$ electrolyte solution (pH 6.8). A syringe pump was used to flow this solution through the channel at a controlled inlet flow rate. Precisely even flow from the two outlet channels was difficult to achieve experimentally as the surface tension of water, combined with the low flow rates needed for laminar flow, prevented the formation of uninterrupted liquid streams from the outlets. An absorbent wicking material was used to counteract the effect of water surface tension such that the force of gravity on the fluid was the dominant factor for droplet formation. This produced a more even flow from the two outlet channels.

A potentiostat (Interface 1000 Gamry) was connected to the foil electrodes to provide a constant current density for the duration of the product generation process. In this 2-elecrode configuration, the applied voltage was typically between 3.8 and 4.5 V. Throughout an experimental run, a steady flow of electrolyte solution was passed through the device. Prior to sample collection, a time span of one and a half residence times was allowed to pass with no current being applied to the system. This served as a purge between testing cycles to flush the channel of residual product from previous trials. After this period, a blank sample was collected for as reference for the HPLC product

analysis. Once blank collection was complete, the current was initiated and another 1.5 residence times were allowed to pass before sample collection. Liquid samples were collected from both outlet channels in pre-weighed vials. Only samples with 50 ± 5% flow to each channel were analyzed for formate content, with 3-5 samples analyzed per test setup (channel width, inlet flow rate). The procedure for sensitive measurement of the formate products is described in the SI.

3. Results and Discussion

The three cells with W = 5, 10, and 15 mm were tested at flow rates between 1 and 20 ml min^{-1}; for a given W, flow rates both above and below the minimum suggested by the dashed line in Fig. 2 were used. The overall FE (both channels) is shown as a function of flow rate in Fig. 6. From a more classical 3-electrode measurement in a membrane-separated cell (see SI), the Sn electrode was found to have a 70% FE to formate at the same current density used in the flow cells. This value is in acceptable agreement with the data in Fig. 6, although the device values are in general lower. It is possible that there is a trend of increasing FE with flow rate, as would be implied by the modelling and by Fig. 2.

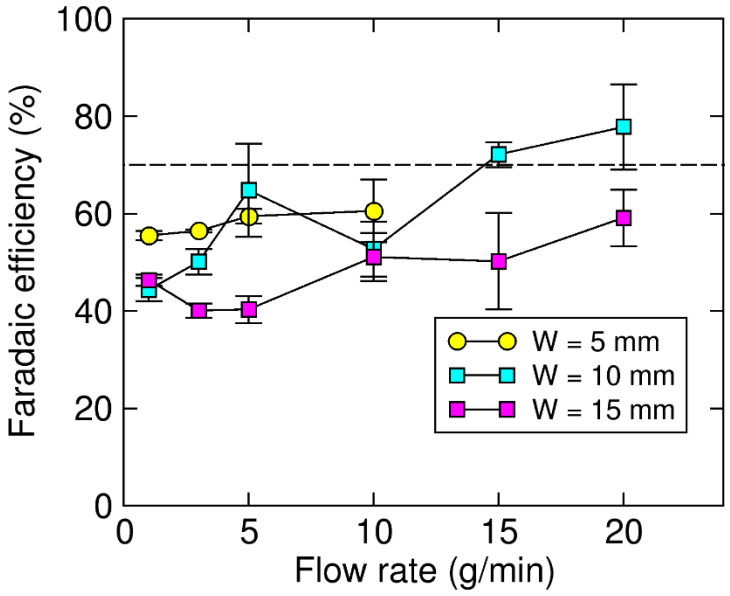

Figure 6. Overall faradaic efficiency (sum of both channels) for formate production in laminar flow reactor operated with 0.1 M $KHCO_3$ electrolyte saturated in CO_2 and a Sn cathode at 5 mA cm^{-2}. Dotted line is the experimentally measured FE in a stirred 3-electrode cell with a Sn cathode.

Separation efficiency is shown as a function of flow rate for W = 5, 10, and 15 mm in Figure 7. For W = 10 and 15 mm at low flow rates, the data follows the predicted trend of increasing separation efficiency with increasing flow rate. The maximum value, 90% is found with W = 15

mm and a flow rate of 3 ml min^{-1}. However, the separation efficiency deceases at higher flow rates. For the narrowest channel, W = 5 mm, the separation efficiency monotonically decreases with flow rate.

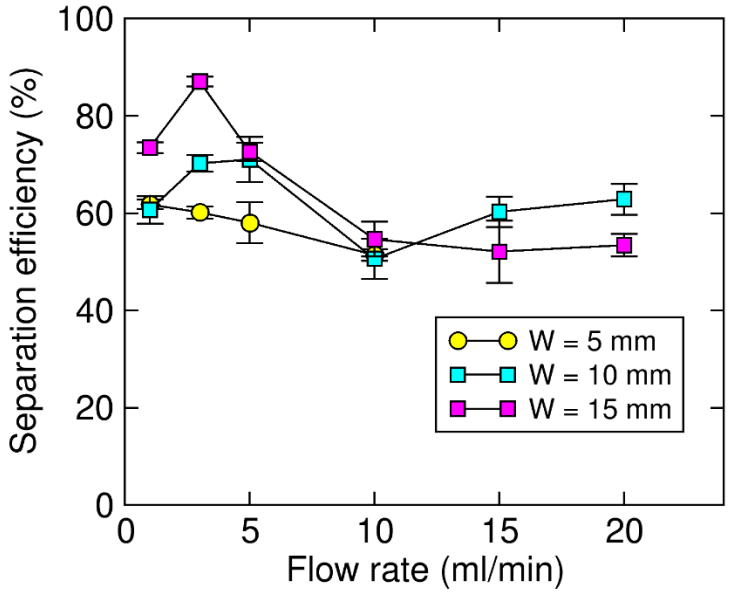

Figure 7. Experimentally measured separation efficiency (Eq. 6) as a function of electrolyte flow rate for channel widths W = 5, 10, and 15 mm. 5 mA cm^{-2}, Sn cathode, Pt anode. 0.1 M $KHCO_3$ electrolyte saturated in CO_2.

We considered a number of factors which would cause the separation efficiency to decline at higher flow rates. While there is greater uncertainty in the measurements at high flow rates due to the lower concentration of the product, the measured values were all at least 10x our detection limit of 1 μM (see SI for calibration procedure). It is possible that the fluid flow is not laminar but has a turbulent component due to the rough surface finish of the 3D printing material This is plausible; however, much of the channel surface is actually the smooth surface of the working and counter electrodes, which would not be expected to yield turbulence at the low Reynolds numbers employed. Bubble formation from hydrogen and oxygen (at the anode) is another possibility. These could lead to turbulence, which would cause additional mixing not considered in the laminar flow model. Faster flow rates could be more likely to develop into turbulent flow when disturbed by bubbles.

4. Conclusions

A one-pass laminar flow reactor for reducing CO_2 to liquid products was designed. Over a wide range of channel dimensions and electrolyte flow rates, efficient separation of the product

stream should be possible assuming the current densities typically achieved with metal cathodes. Prototype reactors were constructed with 3D printing, and their product separation efficiency was evaluated. In general, the experimental separation efficiency was lower than the computationally predicted values and ranged from 52% to 95%, with a maximum found for a 15 mm wide channel and an electrolyte flow rate of 3 ml min^{-1}.

5. Acknowledgments

We thank Karl Walczak and Jacob Gallego for technical help with 3D printing and Meenesh Singh and Kathleen Durkin for helpful discussions regarding COMSOL. This material is based upon work performed by the Joint Center for Artificial Photosynthesis, a DOE Energy Innovation Hub, supported through the Office of Science of the U.S. Department of Energy under Award Number DE-SC0004993. Initial modeling studies were supported by the Singapore Berkeley Initiative for Sustainable Energy (SinBeRISE) which is supported by the National Research Foundation (NRF) of Singapore. We thank the Molecular Graphics and Computation Facility, College of Chemistry, University of California Berkeley, supported by National Science Foundation grant CHE-080405, for providing access to computing resources. Y.L. acknowledges the support of an A*STAR National Science Scholarship.

6. References

[1] Hartmann D L, Tank A M G K and Rusticucci M 2013 Evaluation of Climate Models *Climate Change 2013 - The Physical Science Basis* vol AR5, ed Intergovernmental Panel on Climate Change (Cambridge: Cambridge University Press) pp 741–866

[2] Graves C, Ebbesen S D, Mogensen M and Lackner K S 2011 Sustainable hydrocarbon fuels by recycling CO_2 and H_2O with renewable or nuclear energy *Renew. Sustain. Energy Rev.* **15** 1–23

[3] Chu S and Majumdar A 2012 Opportunities and challenges for a sustainable energy future *Nature* **488** 294–303

[4] Williams J H, DeBenedictis A, Ghanadan R, Mahone A, Moore J, Morrow W R, Price S and Torn M S 2012 The Technology Path to Deep Greenhouse Gas Emissions Cuts by 2050: The Pivotal Role of Electricity *Science* **335** 53–9

[5] Lewis N S 2016 Research opportunities to advance solar energy utilization *Science* **351**aad1920

[6] Listorti A, Durrant J and Barber J 2009 Artificial photosynthesis: Solar to fuel *Nat Mater* **8** 929–30

[7] Hambourger M, Moore G F, Kramer D M, Gust D, Moore A L and Moore T A 2009 Biology and technology for photochemical fuel production *Chem. Soc. Rev.* **38** 25–35

[8] Nocera D G 2012 The artificial leaf. *Acc. Chem. Res.* **45** 767–76

[9] Faunce T A, Lubitz W, Rutherford A W (Bill), MacFarlane D, Moore G F, Yang P, Nocera D G, Moore T A, Gregory D H, Fukuzumi S, Yoon K B, Armstrong F A, Wasielewski M R and Styring S 2013 Energy and environment policy case for a global project on artificial photosynthesis *Energy Environ. Sci.* **6** 695

[10] Rongé J, Bosserez T, Martel D, Nervi C, Boarino L, Taulelle F, Decher G, Bordiga S and Martens J A 2014 Monolithic cells for solar fuels. *Chem. Soc. Rev.* **43** 7963–81

[11] Miller E L 2015 Photoelectrochemical water splitting *Energy Environ. Sci.* **8** 2809–10

[12] Sivula K and van de Krol R 2016 Semiconducting materials for photoelectrochemical energy conversion *Nat. Rev. Mater.* **1** 15010

[13] Nielander A C, Shaner M R, Papadantonakis K M, Francis S A and Lewis N S 2015 A taxonomy for solar fuels generators *Energy Environ. Sci.* **8** 16–25

[14] Ager J W, Shaner M R, Walczak K A, Sharp I D and Ardo S 2015 Experimental demonstrations of spontaneous, solar-driven photoelectrochemical water splitting *Energy Environ. Sci.* **8** 2811–24

[15] Fabian D M, Hu S, Singh N, Houle F A, Hisatomi T, Domen K, Osterloh F E and Ardo S 2015 Particle suspension reactors and materials for solar-driven water splitting *Energy Environ. Sci.* **8** 2825–50

[16] Coridan R H, Nielander A C, Francis S A, McDowell M T, Dix V, Chatman S M and

Lewis N S 2015 Methods for comparing the performance of energy-conversion systems for use in solar fuels and solar electricity generation *Energy Environ. Sci.* **8** 2886–901

[17] Jia J, Seitz L C, Benck J D, Huo Y, Chen Y, Ng J W D, Bilir T, Harris J S and Jaramillo T F 2016 Solar water splitting by photovoltaic-electrolysis with a solar-to-hydrogen efficiency over 30% *Nat. Commun.* **7** 13237

[18] Pinaud B A, Benck J D, Seitz L C, Forman A J, Chen Z, Deutsch T G, James B D, Baum K N, Baum G N, Ardo S, Wang H, Miller E and Jaramillo T F 2013 Technical and economic feasibility of centralized facilities for solar hydrogen production via photocatalysis and photoelectrochemistry *Energy Environ. Sci.* **6** 1983–2002

[19] Zhai P, Haussener S, Ager J, Sathre R, Walczak K, Greenblatt J and McKone T 2013 Net primary energy balance of a solar-driven photoelectrochemical water-splitting device *Energy Environ. Sci.* **6** 2380

[20] Sathre R, Scown C D, Morrow W R, Stevens J C, Sharp I D, Ager J W, Walczak K, Houle F A and Greenblatt J B 2014 Life-cycle net energy assessment of large-scale hydrogen production via photoelectrochemical water splitting *Energy Environ. Sci.* **7** 3264–78

[21] Sathre R, Greenblatt J B, Walczak K, Sharp I D, Stevens J C, Ager J W and Houle F A 2016 Opportunities to improve the net energy performance of photoelectrochemical water-splitting technology *Energy Environ. Sci.* **9** 803–19

[22] Rodriguez C A, Modestino M A, Psaltis D and Moser C 2014 Design and cost considerations for practical solar-hydrogen generators *Energy Environ. Sci.* **7** 3828–35

[23] Kemppainen E, Bodin A, Sebok B, Pedersen T, Seger B, Mei B, Bae D, Vesborg P C K, Halme J, Hansen O, Lund P D and Chorkendorff I 2015 Scalability and feasibility of photoelectrochemical H_2 evolution: the ultimate limit of Pt nanoparticle as an HER catalyst *Energy Environ. Sci.* **8** 2991–9

[24] Lewis N S and Nocera D G 2006 Powering the planet: chemical challenges in solar energy utilization. *Proc. Natl. Acad. Sci. U. S. A.* **103** 15729–35

[25] Pletcher D 2015 The cathodic reduction of carbon dioxide—What can it realistically achieve? A mini review *Electrochem. commun.* **61** 97–101

[26] Armaroli N and Balzani V 2016 Solar Electricity and Solar Fuels: Status and Perspectives in the Context of the Energy Transition *Chem. - A Eur. J.* **22** 32–57

[27] Kelly M J 2016 Lessons from technology development for energy and sustainability *MRS Energy Sustain.* **3** E3

[28] Jhong H-R "Molly," Ma S and Kenis P J 2013 Electrochemical conversion of CO2 to useful chemicals: current status, remaining challenges, and future opportunities *Curr. Opin. Chem. Eng.* **2** 191–9

[29] Ganesh I 2014 Conversion of carbon dioxide into methanol - A potential liquid fuel: Fundamental challenges and opportunities (a review) *Renew. Sustain. Energy Rev.* **31** 221–57

[30] Jones J-P, Prakash G K S and Olah G A 2014 Electrochemical CO_2 Reduction: Recent Advances and Current Trends *Isr. J. Chem.* **54** 1451–66

[31] Qiao J, Liu Y, Hong F and Zhang J 2014 A review of catalysts for the electroreduction of carbon dioxide to produce low-carbon fuels *Chem. Soc. Rev.* **43** 631–75

[32] Kortlever R, Shen J, Schouten K J P, Calle-Vallejo F and Koper M T M 2015 Catalysts and Reaction Pathways for the Electrochemical Reduction of Carbon Dioxide *J. Phys. Chem. Lett.* **6** 4073–82

[33] Arai T, Sato S and Morikawa T 2015 A monolithic device for CO_2 photoreduction to generate liquid organic substances in a single-compartment reactor *Energy Environ. Sci.* **8** 1998–2002

[34] Schreier M, Curvat L, Giordano F, Steier L, Abate A, Zakeeruddin S M, Luo J, Mayer M T and Grätzel M 2015 Efficient photosynthesis of carbon monoxide from CO_2 using perovskite photovoltaics *Nat. Commun.* **6** 7326

[35] Zhou X, Liu R, Sun K, Chen Y, Verlage E, Francis S A, Lewis N S and Xiang C 2016 Solar-Driven Reduction of 1 atm of CO_2 to Formate at 10% Energy-Conversion Efficiency by Use of a TiO_2 -Protected III–V Tandem Photoanode in Conjunction with a Bipolar Membrane and a Pd/C Cathode *ACS Energy Lett.* **1** 764–70

[36] Liu C, Colon B C, Ziesack M, Silver P A and Nocera D G 2016 Water splitting-biosynthetic system with CO_2 reduction efficiencies exceeding photosynthesis *Science* **352** 1210–3

[37] Whipple D T and Kenis P J A 2010 Prospects of CO_2 Utilization via Direct Heterogeneous Electrochemical Reduction *J. Phys. Chem. Lett.* **1** 3451–8

[38] Kelly N and Gibson T 2006 Design and characterization of a robust photoelectrochemical device to generate hydrogen using solar water splitting *Int. J. Hydrogen Energy* **31** 1658–73

[39] Miller E L, Paluselli D, Marsen B and Rocheleau R E 2005 Development of reactively sputtered metal oxide films for hydrogen-producing hybrid multijunction photoelectrodes *Sol. Energy Mater. Sol. Cells* **88** 131–44

[40] Haussener S, Xiang C, Spurgeon J M, Ardo S, Lewis N S and Weber A Z 2012 Modeling, simulation, and design criteria for photoelectrochemical water-splitting systems *Energy Environ. Sci.* **5** 9922

[41] Singh M R and Bell A T 2016 Design of an artificial photosynthetic system for production of alcohols in high concentration from CO_2 *Energy Environ. Sci.* **9** 193–9

[42] Yan X H, Wu R, Xu J B, Luo Z and Zhao T S 2016 A monolayer graphene – Nafion sandwich membrane for direct methanol fuel cells *J. Power Sources* **311** 188–94

[43] Rottiers T, Van Der Bruggen B and Pinoy L 2016 Permeability of Small Alcohols through Commercial Ion-Exchange Membranes Used in Electrodialysis *Ind. Eng. Chem. Res.* **55** 8215–24

[44] Kjeang E, McKechnie J, Sinton D and Djilali N 2007 Planar and three-dimensional

microfluidic fuel cell architectures based on graphite rod electrodes *J. Power Sources* **168** 379–90

[45] Ferrigno R, Stroock A D, Clark T D, Mayer M and Whitesides G M 2002 Membraneless Vanadium Redox Fuel Cell Using Laminar Flow *J. Am. Chem. Soc.* **124** 12930–1

[46] Choban E R, Markoski L J, Wieckowski A and Kenis P J A 2004 Microfluidic fuel cell based on laminar flow *J. Power Sources* **128** 54–60

[47] Chang M-H, Chen F and Fang N-S 2006 Analysis of membraneless fuel cell using laminar flow in a Y-shaped microchannel *J. Power Sources* **159** 810–6

[48] Kjeang E, Djilali N and Sinton D 2009 Microfluidic fuel cells: A review *J. Power Sources* **186** 353–69

[49] Whipple D T, Finke E C and Kenis P J A 2010 Microfluidic Reactor for the Electrochemical Reduction of Carbon Dioxide: The Effect of pH *Electrochem. Solid-State Lett.* **13** B109

[50] Wu K, Birgersson E, Kim B, Kenis P J A and Karimi I A 2014 Modeling and Experimental Validation of Electrochemical Reduction of CO_2 to CO in a Microfluidic Cell *J. Electrochem. Soc.* **162** F23–32

[51] Verma S, Lu X, Ma S, Masel R I and Kenis P J A 2016 The effect of electrolyte composition on the electroreduction of CO_2 to CO on Ag based gas diffusion electrodes *Phys. Chem. Chem. Phys.* **18** 7075–84

[52] Ma S, Sadakiyo M, Luo R, Heima M, Yamauchi M and Kenis P J A 2016 One-step electrosynthesis of ethylene and ethanol from CO_2 in an alkaline electrolyzer *J. Power Sources* **301** 219–28

[53] Hori Y 2008 Electrochemical CO2 Reduction on Metal Electrodes *Modern Aspects of Electrochemistry* Modern Aspects of Electrochemistry ed C G Vayenas, R E White and M E Gamboa-Aldeco (New York, NY: Springer New York) pp 89–189

[54] Hori Y 2008 Electrochemical CO_2 Reduction on Metal Electrodes *Modern Aspects of Electrochemistry* pp 89–189

[55] Bumroongsakulsawat P and Kelsall G H 2015 Tinned graphite felt cathodes for scale-up of electrochemical reduction of aqueous CO2 *Electrochim. Acta* **159** 242–51

[56] Bumroongsakulsawat P and Kelsall G H 2014 Effect of solution pH on CO: formate formation rates during electrochemical reduction of aqueous CO2 at Sn cathodes *Electrochim. Acta* **141** 216–25

[57] Chang M-H, Chen F and Fang N-S 2006 Analysis of membraneless fuel cell using laminar flow in a Y-shaped microchannel *J. Power Sources* **159** 810–6

[58] Goulet M-A and Kjeang E 2014 Co-laminar flow cells for electrochemical energy conversion *J. Power Sources* **260** 186–96

[59] Ismagilov R F, Stroock A D, Kenis P J a., Whitesides G and Stone H a. 2000 Experimental and theoretical scaling laws for transverse diffusive broadening in two-phase laminar flows in microchannels *Appl. Phys. Lett.* **76** 2376

[60] Lobaccaro P, Singh M R, Clark E L, Kwon Y, Bell A T and Ager J W 2016 Effects of temperature and gas–liquid mass transfer on the operation of small electrochemical cells for the quantitative evaluation of CO_2 reduction electrocatalysts *Phys. Chem. Chem. Phys.* **18** 26777–85

[61] Gupta N, Gattrell M and MacDougall B 2006 Calculation for the cathode surface concentrations in the electrochemical reduction of CO_2 in $KHCO_3$ solutions *J. Appl. Electrochem.* **36** 161–72